RSC Advances

PAPER

View Article Online
View Journal | View Issue

Cite this: *RSC Adv.*, 2023, **13**, 10123

Upcycling waste expanded polystyrene into UV-excited dual-mode multicolor luminescent electrospun fiber membranes for advanced anti-counterfeiting†

Yunjie Fan,[ab] Huanyou Su,[b] Pengfei Li,[b] Mingmin Lin,[b] Dan Liu,[*b] Kemei Pei[*a] and Xuebo Cao[*b]

Expanded polystyrene (EPS) is causing severe environmental problems due to its high consumption and non-biodegradability. Upcycling waste EPS into high value-added functional materials is highly advisable in terms of sustainability and environmental concerns. Meanwhile, it is imperative to develop new anti-counterfeiting materials with high security against increasingly high-tech counterfeiting. Developing UV-excited dual-mode luminescent advanced anti-counterfeiting materials that can be excited by commonly used commercial UV light sources (such as 254 nm and 365 nm wavelengths) remains a challenge. Herein, UV-excited dual-mode multicolor luminescent electrospun fiber membranes were fabricated from waste EPS by co-doping with a Eu^{3+} complex and a Tb^{3+} complex *via* electrospinning. The SEM results prove that the lanthanide complexes are uniformly dispersed in the PS matrix. The luminescence analysis results suggest that all the as-prepared fiber membranes with the different mass ratios of the two complexes can exhibit the characteristic emission of Eu^{3+} ions and Tb^{3+} ions under UV light excitation. The corresponding fiber membrane samples can exhibit intense visible luminescence with different colors under UV lights. Moreover, each membrane sample can display different color luminescence irradiated with UV light at 254 nm and 365 nm, respectively, *e.g.* show excellent UV-excited dual-mode luminescent properties. This is owing to the different UV absorption properties of the two lanthanide complexes doped in the fiber membrane. Finally, the fiber membranes with different color luminescence from green light to red light were achieved by tuning the mass ratio of the two complexes in the PS matrix and changing UV irradiation wavelengths. The as-prepared fiber membranes with tunable multicolor luminescence are very promising for high-level anti-counterfeiting applications. This work is very meaningful not only to upcycle waste EPS to high value-added functional products but also to develop advanced anti-counterfeiting materials.

Received 24th January 2023
Accepted 23rd March 2023

DOI: 10.1039/d3ra00509g

rsc.li/rsc-advances

Introduction

Air pollution,[1–4] water pollution[5–8] and solid waste pollution[9–11] are considered three major global environmental issues faced by human beings. One of the main sources of solid waste pollution is discarded plastics. The disposal of plastic waste is currently an urgent environmental concern. Expanded polystyrene (EPS) is one of the most widely used plastics owing to its excellent chemical stability, thermal insulation, simple manufacturing and low cost. The post-consumer EPS is causing serious environmental problems due to its non-biodegradability. Landfilling and incineration are the two most common ways to dispose of waste EPS. However, landfilling is limited by space and can result in the leaching of toxins into the soil and potentially contaminating surface and groundwater, while incineration can release toxic gases dangerous to the environment.[12] Converting waste EPS to recycled products is considered one of the best disposal methods in terms of sustainability and environmental concerns.[13,14] Some functional materials based on waste EPS such as absorption and separation materials for water treatment[15–18] or gas separation,[19,20] and energy storage and conversion materials for supercapacitor and battery applications,[21–24] *etc.* have been reported in the literature. It is very meaningful to develop new high value-added functional materials from waste EPS and investigate their potential applications.

Anti-counterfeiting technologies are crucial for ensuring medicine and food safety, securing currency and valuable

[a]*Department of Chemistry, Zhejiang Sci-Tech University, Hangzhou 310018, China. E-mail: peikemei@zstu.edu.cn*

[b]*College of Biological, Chemical Sciences and Engineering, Jiaxing University, Jiaxing 314001, China. E-mail: liudan@zjxu.edu.cn; xbcao@zjxu.edu.cn*

† Electronic supplementary information (ESI) available. See DOI: https://doi.org/10.1039/d3ra00509g

documents, verifying branded goods, and so on. Against fast-growing counterfeit technologies, intensive research efforts have been made to develop various anti-counterfeiting materials.[25–28] Luminescent anti-counterfeiting materials have attracted considerable attention due to their exceptional luminescent properties under a specific wavelength of light excitation, as well as simple preparation processes, convenient operation and easy identification.[29,30] Different luminescent materials, including organic dyes,[31,32] organic lanthanide complexes,[33,34] inorganic lanthanide nanoparticles,[35,36] carbon dots (CDs),[37,38] perovskite materials,[39,40] *etc.* have been widely investigated and applied in anti-counterfeiting and security fields. Especially, organic lanthanide complexes have drawn extensive attention owing to their intense luminescence, good luminescence stability and long luminescence lifetimes.[41,42] Beyond these advantages, the organic lanthanide complexes also have good compatibility with polymers. The flexible luminescent anti-counterfeiting films or fiber membranes based on polymers can thus be obtained *via* simple doping lanthanide complexes into a polymer matrix, then melt/solution casting or spinning process. Such flexible anti-counterfeiting materials are suitable for industrial large-scale fabrication and construction of luminescence anti-counterfeiting patterns. The lanthanide complexes can be uniformly dispersed and stabilized in the polymer matrix, which can inhibit luminescence quenching caused by the aggregation of the lanthanide ions. Therefore, these flexible polymer luminescent materials not only own the excellent luminescence anti-counterfeiting properties of the lanthanide complexes but also the good mechanical flexibility and processability of the polymers, making them promising in anti-counterfeiting applications. Some luminescent films or fiber membranes containing lanthanide complexes based on polymers, such as PS,[43–45] PVP,[46] PMMA,[47–49] PAN[50,51] and PVA,[52] *etc.* have been investigated and shown potential for the anti-counterfeiting and information encryption applications. However, these luminescent materials can only emit a single color under a specific wavelength of light (called single-mode luminescence) and are relatively easy to counterfeit. They can no longer be against continuously growing high-tech counterfeiting. Hence, it is very necessary to develop new lanthanide complexes based on polymers with higher anti-counterfeiting security.

Dual-mode luminescent materials are a kind of advanced anti-counterfeiting materials that can exhibit different color luminescence under two different wavelength lights (ultraviolet (UV) and/or near-infrared (NIR) lights), making it very difficult to falsify in the practical application. Growing efforts have been devoted to developing dual-mode luminescent materials to satisfy high-level anti-counterfeiting requirements.[53–60] Although these dual-mode luminescent materials reported in the literature have better anti-counterfeiting security than traditional single-mode luminescent materials, most of them need NIR light sources as excitation sources.[53–57] Relative to NIR light sources, UV light sources are cost-effective, commercially readily available and easy to operate (especially hand-held 254 nm and 365 nm UV lamps).[58,59] Accordingly, designing UV-excited dual-mode luminescent materials that only need UV excitation light sources would be more promising in practical anti-counterfeiting applications.

Nevertheless, there are only a few reports on UV-excited dual-mode luminescent materials. For example, Chen *et al.* designed and prepared a kind of UV-switchable hybrid fluorescent inks and polymer (polyvinyl alcohol) composite films based on the lanthanide complexes $[Eu(DPA)_3]^{3-}$ and CDs prepared from methacrylic acid and *m*-phenylenediamine. Both the obtained security ink and films can display intense green and red luminescence under 365 nm and 254 nm UV light, respectively.[60] Li *et al.* developed a UV light-switchable (254 nm and 365 nm) luminescent composite prepared using CDs based on citric acid and ethanediamine and lanthanide nanoparticles Y_2O_3:Eu for anti-counterfeiting applications.[59] To achieve the dual-mode luminescent anti-counterfeiting function, different types of luminescence components, including organic lanthanide complexes, inorganic lanthanide nanoparticles and CDs, were introduced in these luminescent materials reported. However, these different kinds of luminescence components usually have very different luminescence properties, such as emission bandwidth, intensities and lifetimes, and so on. These luminescence property differences lead it not easy to adjust the luminescent properties of the obtained anti-counterfeiting materials. The use of the same type of luminescence components with similar luminescence properties would make it easier to fine-tune the emission colors of the prepared dual-mode luminescent materials and construct the anti-counterfeiting patterns. The organic lanthanide complexes have many excellent luminescence properties mentioned above, *e.g.* strong emission, excellent luminescence stability, long luminescence lifetimes and good compatibility with polymers. Europium (Eu^{3+}) complexes and terbium (Tb^{3+}) complexes are two kinds of the most popular lanthanide complexes because they can display bright red and green luminescence visible to the naked eye under UV light, respectively.

Based on the above concerns, an effective method for fabricating UV-excited dual-mode multicolor luminescent fiber membranes from waste EPS for advanced anti-counterfeiting *via* electrospinning technique was developed in this work (Fig. 1). In these fiber membranes, recycled PS with excellent solubility and spinnability was used as the polymer matrix, wherein a Eu^{3+} complex and a Tb^{3+} complex were doped as luminescence components to realize UV-excited dual-mode emission. By tuning the mass ratio of the two complexes in the PS matrix, the fiber membranes with intense multicolor luminescence were obtained. Moreover, each fiber membrane can emit different color lights under two different wavelengths of UV light sources (254 nm and 365 nm light), respectively. Especially, the obtained PS–Eu_1–Tb_{60} fiber membrane with the mass ratio of the Eu^{3+} complex and the Tb^{3+} complex of 1 : 60 can exhibit intense green and red lights upon excitation with 254 nm and 365 nm UV light, respectively. The anti-counterfeiting patterns with high security based on the as-prepared fiber membranes were also designed. The UV-excited dual-mode luminescence properties and mechanism of the as-prepared fiber membranes were studied by analyzing their UV-vis absorption, excitation and emission spectra. The aim of

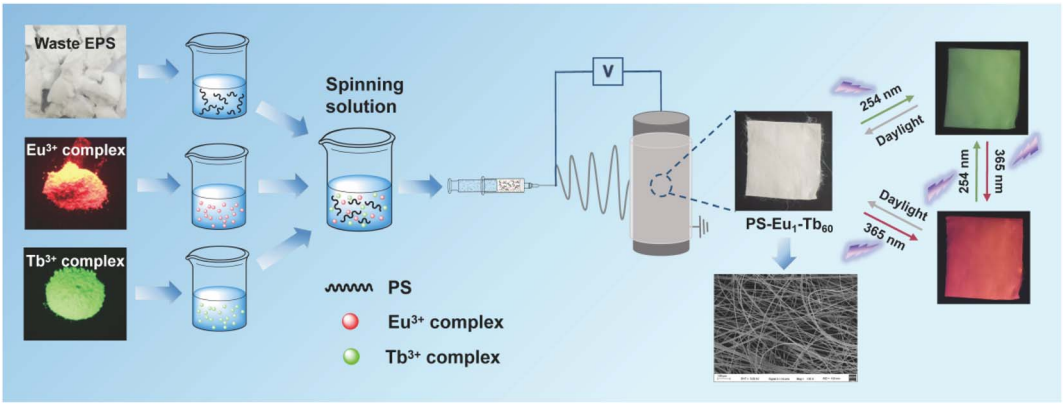

Fig. 1 Fabrication illustration of the UV-excited dual-mode luminescent anti-counterfeiting electrospun fiber membranes from waste EPS.

this work lies in developing new value-added dual-mode luminescent functional membranes for advanced anti-counterfeiting from the perspective of upcycling waste EPS. To the best of our knowledge, UV-excited dual-mode luminescent anti-counterfeiting functional materials from waste EPS have not been reported so far.

Materials and methods

Materials

PS was recycled from the used product-packaging EPS. The recycling process of EPS and the characterization of the recycled PS are described in the ESI.† The Eu^{3+} complex and the Tb^{3+} complex were prepared using different β-diketone ligands. 2-Thenoyltrifluoroacetone (TTA) was as the ligand of the Eu^{3+} ions in the Eu^{3+} complex. Acetylacetone (AcAc) was as the ligand of the Tb^{3+} ions in the Tb^{3+} complex. 1,10-Phenanthroline (Phen) was as the synergetic ligand of the Eu^{3+} or Tb^{3+} ions in both two complexes. The synthesis and characterization of the two complexes are described in the ESI† in detail. *N*,*N*-Dimethylformamide (DMF) was purchased from Sinopharm Chemical Reagent Co., Ltd.

Fabrication of the UV-excited dual-mode luminescent electrospun fiber membranes

The UV-excited dual-mode luminescent electrospun fiber membranes were prepared *via* an electrospinning apparatus (SS-3556H) supplied by Beijing Ucalery Technology and Development Co., Ltd. by the following process. 2.5000 g of the recycled PS was dissolved in 5.5 mL DMF. 0.2500 g of the mixture powder of the Eu^{3+} complex and the Tb^{3+} complex was dissolved in 2.5 mL DMF. The mass ratio of the Eu^{3+} complex and the Tb^{3+} complex in the mixture powder was 1 : 3, 1 : 10, 1 : 20, 1 : 50, 1 : 60, 1 : 70 and 1 : 150, respectively. The obtained complex solution was added to the PS solution to yield a homogeneous electrospinning solution by vigorous stirring. The mass percentage of the lanthanide complexes in the PS matrix was 10 wt%. The obtained electrospinning solution was then poured into a 10 mL plastic syringe with a stainless-steel needle with an inner diameter of 0.5 mm. During electrospinning, the applied voltage was 20 kV, and the syringe was pushed at the speed of 0.2 mm min^{-1}. The electrospun fiber membranes were collected on a metallic roller wrapped with aluminum. The distance between the collection plate and the needle of the syringe was 15 cm. The collected fiber membranes were dried at 60 °C for 12 h in a vacuum oven. The obtained fiber membranes were named as the PS–Eu_1–Tb_3, PS–Eu_1–Tb_{10}, PS–Eu_1–Tb_{20}, PS–Eu_1–Tb_{50}, PS–Eu_1–Tb_{60}, PS–Eu_1–Tb_{70} and PS–Eu_1–Tb_{150} fiber membrane, respectively.

For comparison, two single-doped fiber membranes were also prepared under similar conditions by replacing the mixture powder of the Eu^{3+} complex and Tb^{3+} complex with the Eu^{3+} complex or the Tb^{3+} complex, respectively. The obtained fiber membranes were named as the PS–Eu fiber membrane and the PS–Tb fiber membrane, respectively. Besides, the neat PS fiber membrane was also prepared by similar conditions.

Characterization

The morphology and elemental mapping were obtained by using a ZEISS Sigma 500 Scanning Electron Microscope (SEM) with an OXFORD extreme 65 energy dispersive spectrometer. The ultraviolet-visible (UV-vis) absorption spectra were measured by a PerkinElmer Lambda 35 UV/vis spectrophotometer at room temperature. The luminescence excitation and emission spectra were measured on a Hitachi F-4600 fluorescence spectrophotometer. Digital images were taken using a Nikon camera.

Results and discussion

Morphologies of the UV-excited dual-mode luminescent electrospun fiber membranes

The morphologies of the as-prepared UV-excited dual-mode luminescent electrospun fiber membranes were investigated by SEM. The results suggested that the fiber membrane samples with the different mass ratios of the Eu^{3+} complex and the Tb^{3+} complex show similar morphologies. Fig. 2a and c present the SEM images of the PS–Eu_1–Tb_{60} fiber membrane. The fiber diameters in the PS–Eu_1–Tb_{60} fiber membrane are found to be in the range of 3 to 5 μm. In comparison to the neat PS fiber

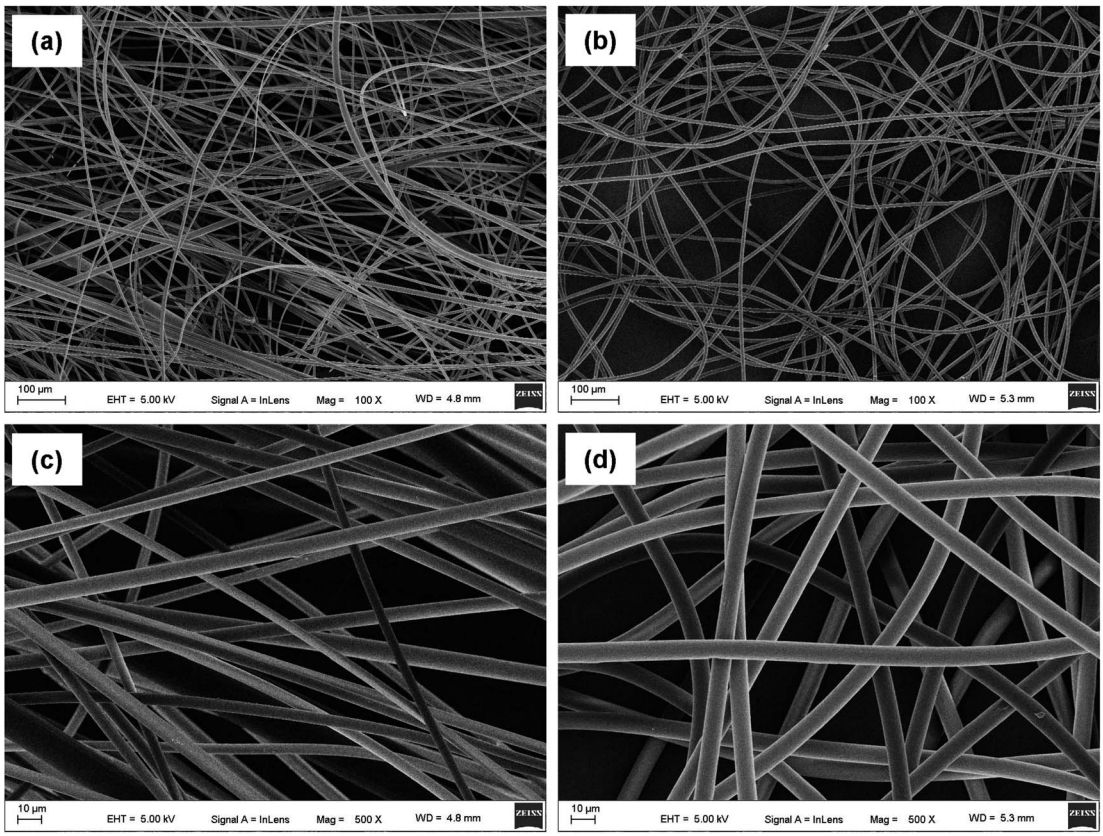

Fig. 2 SEM images of the PS–Eu_1–Tb_{60} fiber membrane (a and c) and the neat PS fiber membrane (b and d).

membrane (Fig. 2b and d), the PS–Eu_1–Tb_{60} fiber membrane has slightly smaller fiber diameters, which is due to the presence of the lanthanide complexes leading to an increase of excess charge density in the electrospinning fibers.[61,62] The fiber surfaces of the PS–Eu_1–Tb_{60} fiber membrane are smooth without microscopically identifiable particles, suggesting that the lanthanide complexes are uniformly dispersed in the PS matrix. The elemental mappings of the PS–Eu_1–Tb_{60} fiber membrane were also performed as shown in Fig. 3. The magenta, cyan, blue, yellow, red, and green colors correspond to the mapping of C, N, O, F, Eu and Tb elements, respectively. The results suggest that the Eu^{3+} complex and Tb^{3+} complex were successfully doped into the PS fibers. Furthermore, it can be seen from the overlay image that the distribution ranges of these elements are well overlapped, confirming that the doping of the Eu^{3+} complex and Tb^{3+} complex are uniform in the fiber matrix.

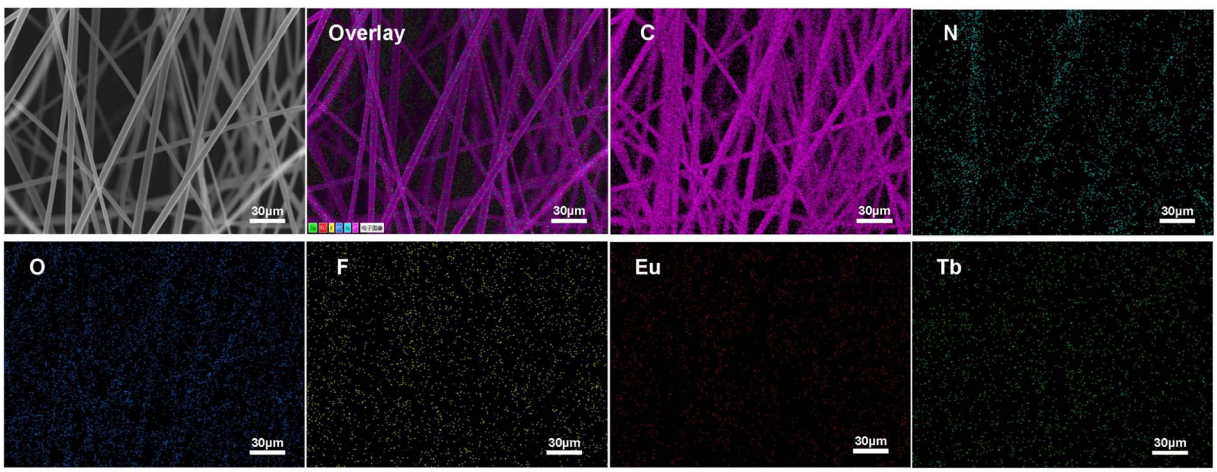

Fig. 3 Elemental mapping images of the PS–Eu_1–Tb_{60} fiber membrane.

Luminescence properties of the UV-excited dual-mode luminescent electrospun fiber membranes

The UV-excited dual-mode luminescence properties of the as-prepared electrospun fiber membranes were investigated. Fig. 4a and c exhibit the emission spectra of the fiber membranes under 254 nm and 365 nm excitation, respectively. It can be seen that all the fiber membranes can emit characteristic luminescence of both Eu^{3+} ions and Tb^{3+} ions under 254 nm or 365 nm irradiation. Among the characteristic emission peaks of the Tb^{3+} ions, the peak at 546 nm attributed to the $^5D_4 \rightarrow {}^7F_5$ transitions of Tb^{3+} ions is the strongest, corresponding to the green light. Among the emission peaks of the Eu^{3+} ions, the peak at 617 nm ascribed to the $^5D_0 \rightarrow {}^7F_2$ transition of Eu^{3+} ions is the strongest, corresponding to the red light. With the increase of the mass ratio of the Tb^{3+} complex and the Eu^{3+} complex in the fiber membranes (from PS–Eu_1–Tb_3 to PS–Eu_1–Tb_{150}), the intensities of the Tb^{3+} emission peaks gradually enhance, while the intensities of the Eu^{3+} emission peaks gradually decrease. Such change tendency can be visually observed from the change of the emission intensity ratios at 546 nm of the Tb^{3+} ions and 617 nm of the Eu^{3+} ions of the different fiber membranes, as shown in the insets in Fig. 4a and c. The results indicate that the fiber membranes with different the mass ratio of the Tb^{3+} complex and the Eu^{3+} complex can exhibit different color lights. Noteworthy, as for the same fiber membrane sample, the relative intensities of the Tb^{3+} emission peaks and the Eu^{3+} emission peaks under different excitation wavelengths (254 nm and 365 nm) are different. Take the PS–Eu_1–Tb_{60} fiber membrane as an example, the peak at 546 nm corresponding to the green light of the Tb^{3+} ions is strongest excited by 254 nm light as shown in Fig. 4a, whereas the peak at 617 nm corresponding to the red light of the Eu^{3+} ions is strongest excited by 365 nm light as displayed in Fig. 4c. These results suggest that 254 nm excitation light is benefited for the emission of the Eu^{3+} ions, while 365 nm excitation light is benefited for the emission of the Tb^{3+} ions. The reason for this will be discussed later in this work. The results also indicate that the as-prepared fiber membranes can emit different color lights excited by different wavelength UV lights, *e.g.* possess UV-excited dual-mode emission properties.

To confirm the above deduction, the emission colors of these fiber membranes were further analyzed by the CIE chromaticity diagram. The results are shown in Fig. 4b and d, in which the CIE coordinates of the fiber membranes were calculated based on their corresponding emission spectra in Fig. 4a and c. It can

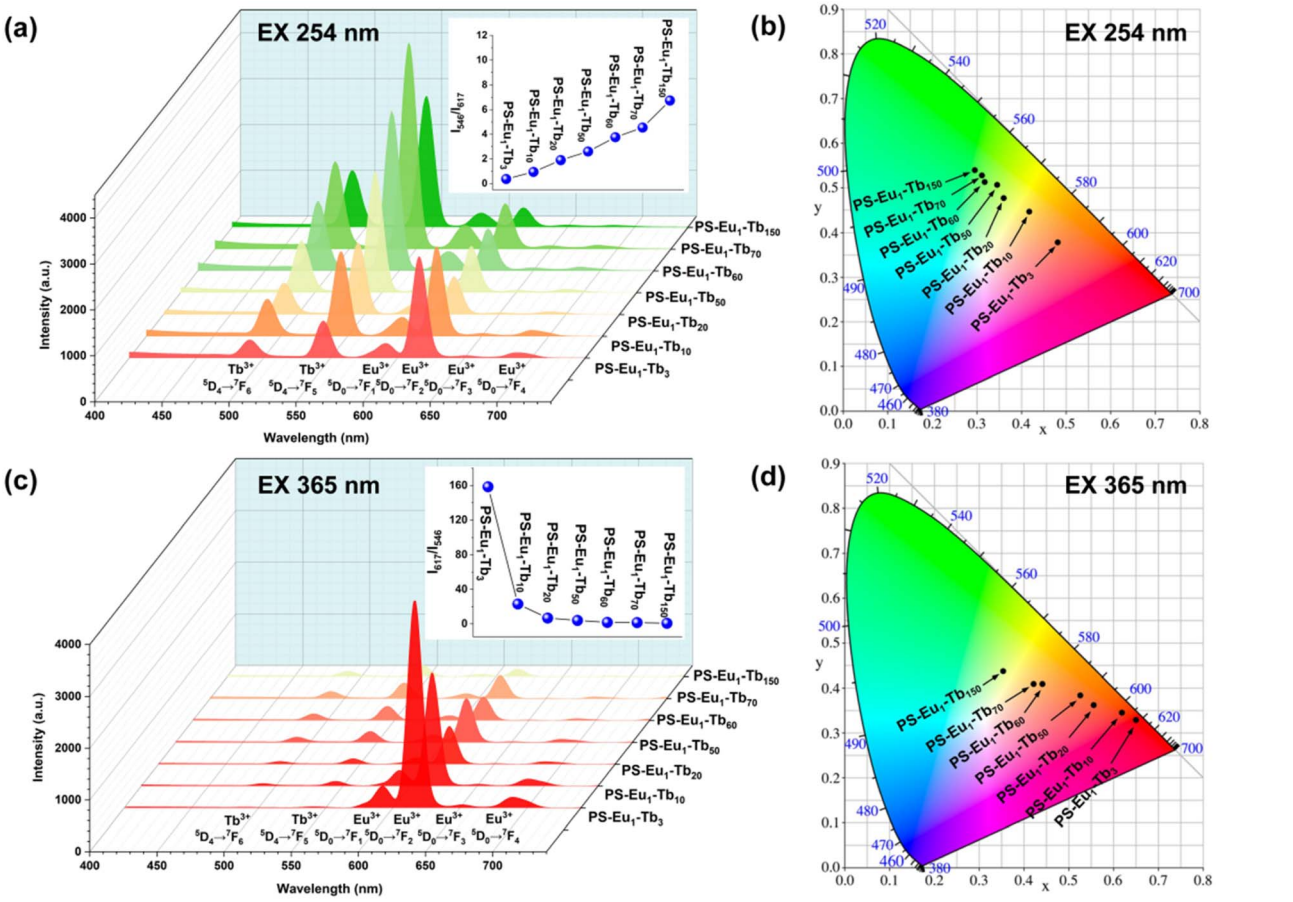

Fig. 4 Emission spectra and CIE chromaticity diagrams of the UV-excited dual-mode luminescent electrospun fiber membranes under 254 nm (a and b) and 365 nm (c and d) excitation, respectively. The insets are the emission intensity ratios at 546 nm and 617 nm of the dual-mode luminescent electrospun fiber membranes.

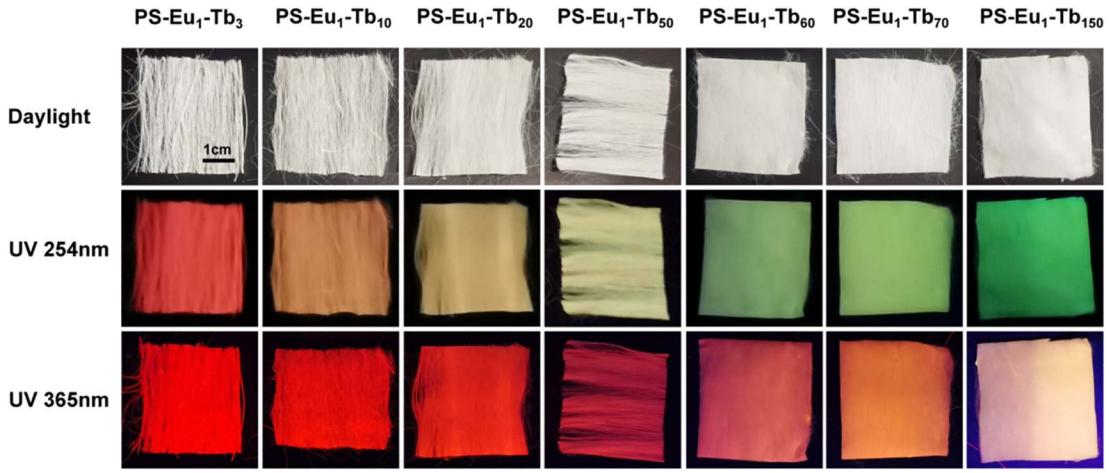

Fig. 5 Digital images of the UV-excited dual-mode luminescent electrospun fiber membranes under daylight, 254 nm light and 365 nm light, respectively.

be seen that with the increase of the mass ratio of the Tb^{3+} complex and the Eu^{3+} complex in the fiber membranes, the coordinate points of the fiber membranes in CIE chromaticity diagram gradually shifted from orange-red to green region upon excitation with 254 nm, while the coordinate points in CIE chromaticity diagram shifted gradually from red to light yellow region upon excitation with 365 nm. The digital images of the as-prepared fibers under daylight, 254 nm light and 365 nm light are presented in Fig. 5. It can be observed that all the fiber membrane samples are white under daylight. Under the hand-held 254 nm or 365 nm UV lamp, the fiber membrane samples display different lights, respectively. Especially, the PS–Eu_1–Tb_{60} fiber membrane can emit two lights close to green and red primary colors under 254 nm and 365 nm light excitation, respectively, which are easily discriminated by the naked eye. Additionally, it is found that such luminescence properties of the as-prepared fiber membranes are reversible. Fig. 1 shows the reversible luminescence properties of the PS–Eu_1–Tb_{60} fiber membrane.

Based on the reversible UV-excited dual-mode multicolor luminescence properties of these fiber membranes, diverse anti-counterfeiting or encryption patterns can be designed. For instance, Fig. 6 shows the schematic illustrations of the dual-mode anti-counterfeiting designs of the "shamrock" and "colorful stripes" based on the as-prepared different fiber membranes. As shown in Fig. 6a, the "shamrock" is constructed using the three fiber membranes (*e.g.* PS–Eu_1–Tb_{10}, PS–Eu_1–Tb_{60} and PS–Eu_1–Tb_{150}). The "shamrock" is white under daylight, whereas exhibits multicolor luminescence under 245 nm or 365 nm light. Moreover, each leaf of the "shamrock" can emit different color lights under two different excitation lights (245 nm and 365 nm), respectively. That is, the color of the "shamrock" can switch by adjusting the excitation light sources, making it not easy to falsify. The "colorful stripes" in Fig. 6b is constructed using the seven different fiber membranes (*e.g.* PS–Eu_1–Tb_3, PS–Eu_1–Tb_{10}, PS–Eu_1–Tb_{20}, PS–Eu_1–Tb_{50}, PS–Eu_1–Tb_{60}, PS–Eu_1–Tb_{70} and PS–Eu_1–Tb_{150}). The "colorful stripes" also shows the white color under daylight. When excited by UV lights with different wavelengths, the "colorful stripes" can display complex multicolor luminescence, showing a high-level anti-counterfeiting function. Noteworthy, these fiber membranes also have good flexibility and can be directly attached to different substrates for the anti-counterfeiting applications. As shown in Fig. 7a–c, the fiber membranes with various emission colors can be used as luminescent anti-counterfeiting labels by attaching them to the sock, computer mouse or wine bottle. Such anti-counterfeiting labels clearly show different luminescence colors under daylight, 254 nm light and 365 nm light, respectively, that are easily recognized by the naked eye.

In summary, the advantages of the dual-mode luminescent electrospun fiber membranes prepared from waste EPS in this work can be summarized as follows: low cost (the polymer matrix from plastic waste), easily recognizable colors by the naked eye, tunable multicolor luminescence, common cost-effective light sources in the market (*e.g.* hand-held 254 nm and 365 nm UV light sources), excellent flexibility. Therefore, these UV-excited dual-mode luminescent fiber membranes would be very promising in advanced anti-counterfeiting and information encryption practical applications.

Luminescence mechanism of the UV-excited dual-mode luminescent electrospun fiber membranes

To investigate the specific UV-excited dual-mode luminescent function of the as-prepared fiber membranes, the luminescence properties of the PS–Eu fiber membrane and the PS–Tb fiber membrane were first investigated. Fig. 8 presents the emission spectra of the PS–Eu fiber membrane and the PS–Tb fiber membrane under 254 nm and 365 nm excitation, respectively. It can be seen that both of them can emit the characteristic luminescence from the Eu^{3+} ions and the Tb^{3+} ions upon 254 nm and 365 nm irradiation, respectively. However, the emission intensities of the PS–Eu fiber membrane under 365 nm excitation are much higher than that under 254 nm

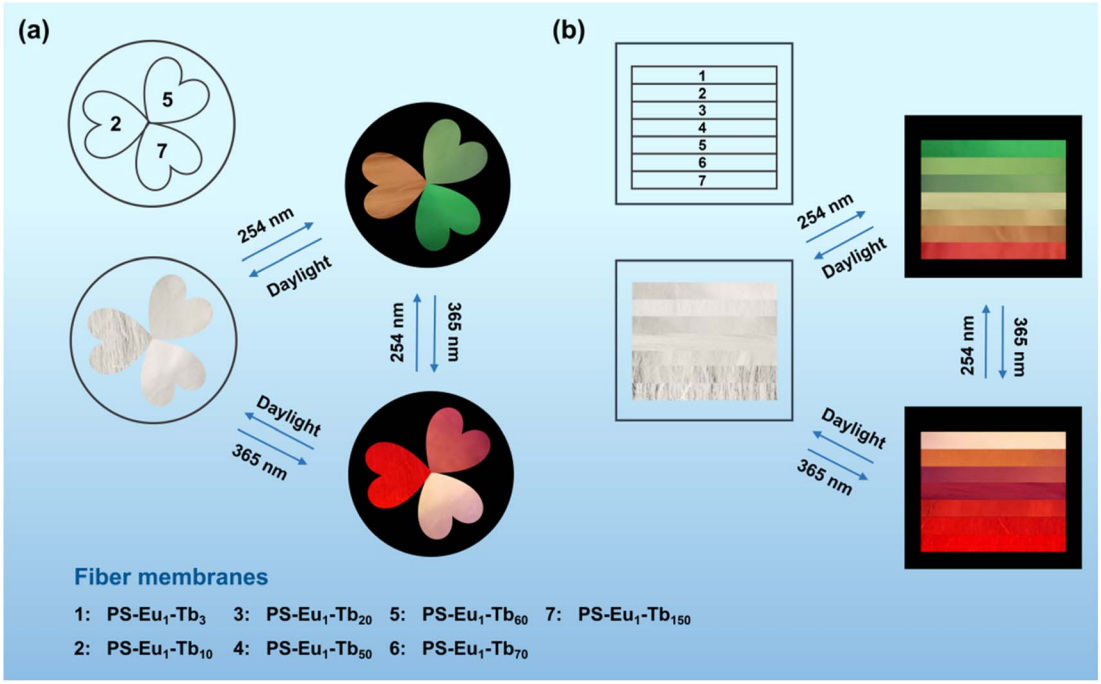

Fig. 6 Schematic illustration of the anti-counterfeiting designs using the UV-excited dual-mode luminescent electrospun fiber membranes. (a) "Shamrock" and (b) "colorful stripes" under daylight, 254 nm light and 365 nm light, respectively.

excitation (Fig. 8a and b), while the emission intensity of the PS–Tb fiber membrane under 254 nm excitation is much higher than that under 365 nm excitation (Fig. 8c and d). As a result, the PS–Eu membrane sample shows stronger red light irradiated with 365 nm light than with 254 nm light, as shown in the insets Fig. 8a and b. The PS–Tb membrane sample displays stronger green light excited by 254 nm light than by 365 nm light, as exhibited in the insets in Fig. 8c and d.

To explore the reasons for this, the UV-vis absorption and the excitation spectra of both the PS–Eu fiber membrane and the PS–Tb fiber membrane were further investigated. Fig. 9a shows the excitation spectrum monitored with 620 nm corresponding to the $^5D_0 \rightarrow {}^7F_2$ transition of the Eu^{3+} ions of the PS–Eu fiber membrane. Fig. 9b presents the UV-vis absorption spectrum of the PS–Eu fiber membrane. It can be observed that the excitation band at 275–415 nm (centered at 375 nm) of the PS–Eu fiber membrane in Fig. 9a is well overlapped with the corresponding UV absorption

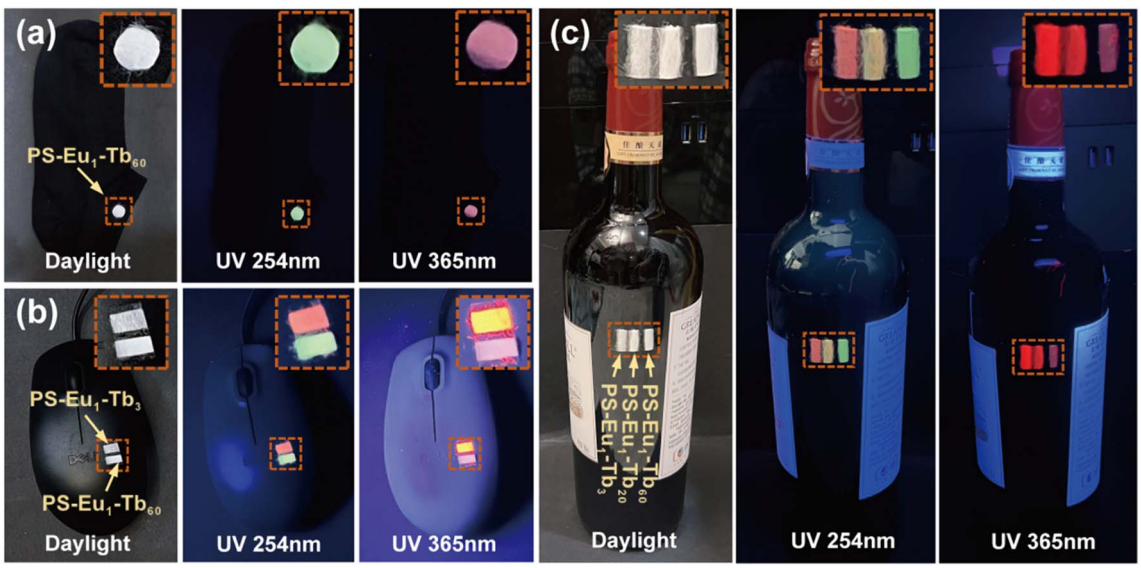

Fig. 7 Anti-counterfeiting applications of the UV-excited dual-mode luminescent electrospun fiber membranes in a sock (a), computer mouse (b) and wine bottle (c).

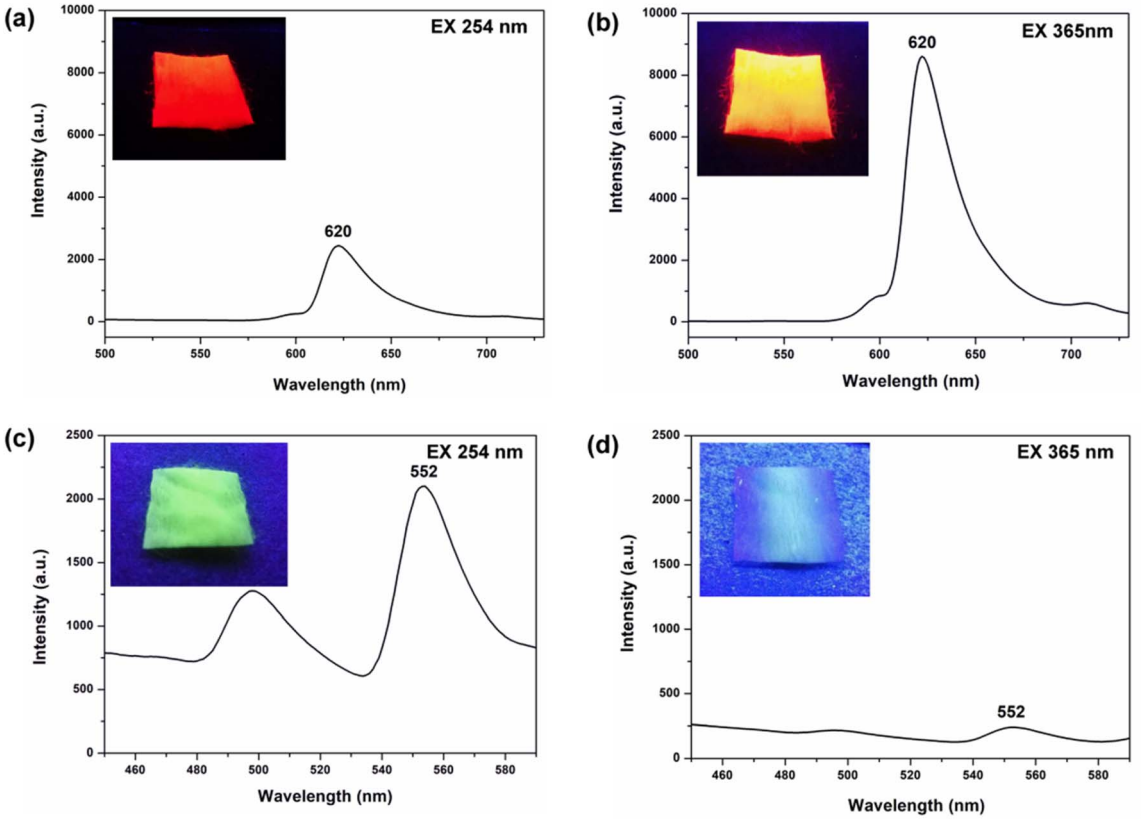

Fig. 8 Emission spectra of the PS–Eu fiber membrane (a and b) and the PS–Tb fiber membrane (c and d) under 254 nm and 365 nm excitation, respectively. The insert figures are the digital images of the PS–Eu fiber membrane and the PS–Tb fiber membrane under 254 nm light and 365 nm light, respectively.

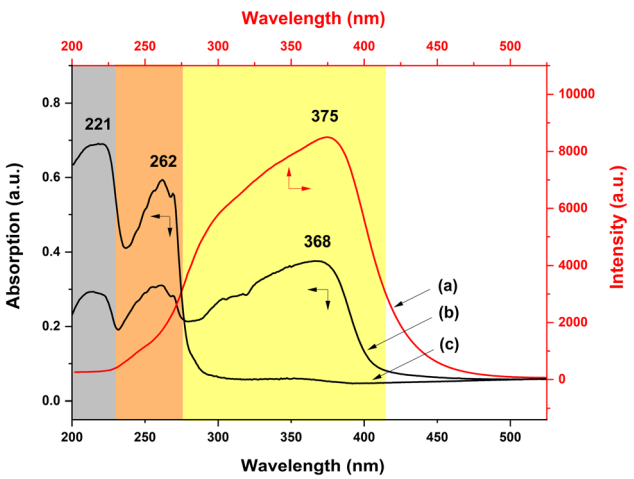

Fig. 9 Excitation (a) and UV-vis absorption (b) spectra of the PS–Eu fiber membrane and UV-vis absorption spectrum (c) of the neat PS fiber membrane.

band at 280–410 nm (centered at 368 nm) in Fig. 9b. The absorption band at the long wavelength centered at 368 nm is mainly from the UV absorption of the organic ligand TTA of the Eu^{3+} complex in the PS–Eu fiber membrane.[63–65] The results indicate that the energy transfer could occur predominantly from the TTA ligand to the Eu^{3+} ions in the PS–Eu fiber membrane.

As is well known, a good energy match between a ligand and lanthanide ions is crucial to sensitize lanthanide ions, and as a result achieve strong luminescence emission.[66] According to Latva's empirical rule, a suitable energy difference (ΔE) between the lowest triplet level ($^3\pi\pi^*$) of a ligand and the resonant energy level of the lanthanide ion is needed to realize an effective ligand-to-lanthanide energy transfer process.[67] For the Eu^{3+} ion, the optimal energy difference ($\Delta E = {}^3\pi\pi^* - {}^5D_0$) is assumed to exist around 2500–4000 cm^{-1}.[68] The resonant energy level of the Eu^{3+} ion $^5D_0$ is known be 17 300 cm^{-1}.[68,69] The lowest triplet energy level ($^3\pi\pi^*$) of TTA and Phen are about 20 400 cm^{-1} and 22 100 cm^{-1}, respectively.[51,70,71] For TTA and Phen, the obtained energy difference ($\Delta E = {}^3\pi\pi^* - {}^5D_0$) by calculation are 3100 cm^{-1} and 4800 cm^{-1}, respectively. The former ΔE is within the optimal energy gap of 2500–4000 cm^{-1}, while the latter ΔE is out of the range of 2500–4000 cm^{-1}. Therefore, relative to Phen, TTA is more suitable for sensitizing Eu^{3+} ions, which is consistent with the conclusion in the literature.[51] Besides, the UV-vis absorption spectrum of the neat PS fiber membrane was also investigated for comparison. As shown in Fig. 9c, the two UV absorption bands of PS (peaked at 221 nm and 262 nm, respectively) are not observed in Fig. 9a. The result suggests that the luminescence of the PS–Eu fiber membrane is mainly sensitized by the organic ligand rather than by the polymer matrix. Here, it is noteworthy that the

maximum excitation peak of the PS–Eu fiber membrane located at 375 nm (Fig. 9a) is near 365 nm. This is just the reason why the PS–Eu fiber membrane shows a more intense emission peak at 620 nm and its membrane sample displays stronger red light under 365 nm light than under 254 nm light (Fig. 8b).

On the other hand, the UV-vis absorption and the excitation spectra of the PS–Tb fiber membrane were also investigated. Fig. 10a exhibits the UV-vis absorption spectrum of the PS–Tb fiber membrane. It can be found that the fiber membrane displays a quite broad absorption band at 200–370 nm (centered at 271 nm), which could be an overlapping absorption band of the PS matrix and the organic ligands (AcAc and Phen). Fig. 10b presents the excitation spectrum monitored with the 552 nm emission corresponding to the $^5D_4 \rightarrow {}^7F_5$ transition of the Tb^{3+} ions of the PS–Tb fiber membrane. Compared with the absorption band of the PS–Tb fiber membrane (Fig. 10a), its excitation band (Fig. 10b) becomes narrower. It locates at 250–370 nm with a sharp peak at 281 nm and a shoulder peak at about 320 nm, which are mainly ascribed to the UV absorption of the organic ligands Phen and AcAc, respectively.[63,64,72] Hence, it can be deduced that the Tb^{3+} emission of the PS–Tb fiber membrane might be from the synergistic sensitization effect of AcAc and Phen.

The energy transfer process in the PS–Tb fiber membrane was further investigated. For the Tb^{3+} ion, the optimal energy difference ($\Delta E = {}^3\pi\pi^* - {}^5D_4$) is considered to be around 2500–4500 cm^{-1} according to Latva's empirical rule.[67,68] The resonant energy level of the Tb^{3+} ion $^5D_4$ is known be 20 500 cm^{-1}.[69] The lowest triplet energy level ($^3\pi\pi^*$) of AcAc is about 25 310 cm^{-1}.[73,74] The energy difference ($\Delta E = {}^3\pi\pi^* - {}^5D_4$) between AcAc and Tb^{3+} ions is calculated to be 4810 cm^{-1}, which is closer to the optimal energy difference. Thus, AcAc can transfer energy to the Tb^{3+} ions in the PS–Tb fibers, which is also proved in the previous literature.[65,73] On the other hand, the energy difference ($\Delta E = {}^3\pi\pi^* - {}^5D_4$) between Phen and Tb^{3+} ions calculated is 1600 cm^{-1}. Although the energy difference is smaller than the optimal energy difference, the energy transfer from Phen to Tb^{3+} ions can still occur, merely that an energy back transfer from the Tb^{3+} ions to Phen may take place.[66,75,76] Accordingly, it can be concluded that the characteristic emission of the Tb^{3+} ions in the PS–Tb fiber membrane is due to the synergistic sensitization of the two ligands (AcAc and Phen). Noteworthy, different from the PS–Eu fiber membrane, the maximum excitation peak of the PS–Tb fiber membrane at 281 nm (Fig. 10b) is near 254 nm. Therefore, the PS–Tb fiber membrane shows a higher emission peak at 552 nm and its membrane sample exhibits stronger green light under 254 nm light than under 365 nm light (Fig. 8c). So far, quite understandably, the fundamental reason for different emission intensities of the PS–Eu fiber membrane and the PS–Tb fiber membrane under different wavelengths of UV lights is that the UV absorption wavelengths of the organic ligands (*e.g.* TTA, Phen and AcAc) sensitizing to the lanthanide ions are different.

To investigate deeply the UV-excited dual-mode luminescence behaviors of the as-prepared dual-mode luminescent electrospun fiber membranes, the UV-vis absorption and excitation spectra of the fiber membranes were further investigated. Fig. 11a shows the UV-vis absorption spectrum of the PS–Eu_1–Tb_{60} fiber membrane. The absorption spectra of the PS–Tb fiber membrane and the PS–Eu fiber membrane are also presented in Fig. 11b and c, respectively, for comparison. It can be seen from Fig. 11a that the PS–Eu_1–Tb_{60} fiber membrane displays a strong absorption band at 200–335 nm (centered at 270 nm) and a shoulder band at 335–400 nm (centered at about 365 nm), respectively. These two absorption bands overlap well with the main UV absorption band of the PS–Tb fiber membrane (Fig. 11b) and the PS–Eu fiber membrane (Fig. 11c), respectively. It is evident that the two bands of the PS–Eu_1–Tb_{60} fiber membrane are mainly from the UV absorption of the Tb^{3+} complex and the Eu^{3+} complex doped in the PS–Eu_1–Tb_{60} fiber membrane, respectively. This result also proves that the mixture of the two lanthanide complexes in the fiber membrane has little effect on their respective UV absorption properties.

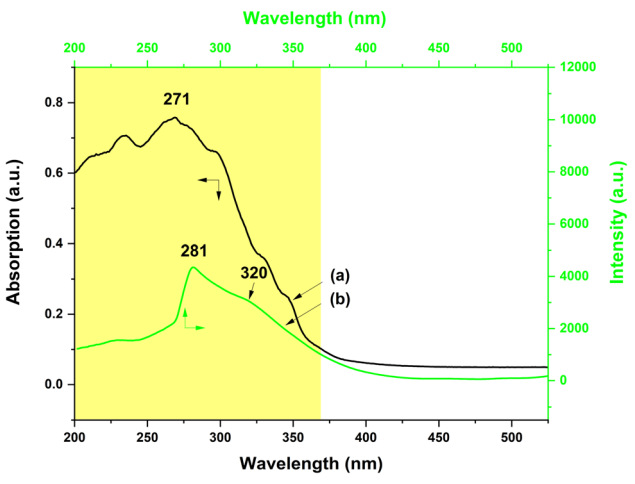

Fig. 10 UV-vis absorption (a) and excitation (b) spectra of the PS–Tb fiber membrane.

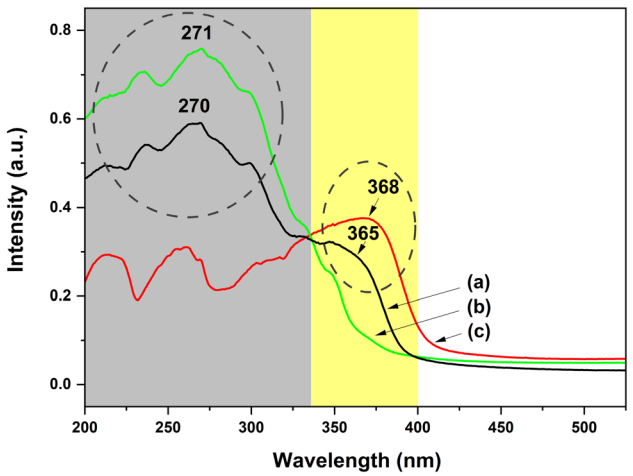

Fig. 11 UV-vis absorption spectra of the PS–Eu_1–Tb_{60} fiber membrane (a), the PS–Tb fiber membrane (b) and the PS–Eu fiber membrane (c).

Fig. 12a and b show the excitation spectra of the PS–Eu_1–Tb_{60} fiber membrane by monitoring the maximum emission peak of the Tb^{3+} ions at 546 nm ($^5D_4 \rightarrow {}^7F_5$ transition) and the maximum emission peak of the Eu^{3+} ions at 617 nm ($^5D_0 \rightarrow {}^7F_2$ transition) of the PS–Eu_1–Tb_{60} fiber membrane (Fig. 4a and c), respectively. It can be observed from Fig. 12a that when monitoring the Tb^{3+} emission at 546 nm, the PS–Eu_1–Tb_{60} fiber membrane displays an excitation band at 240–350 nm with a peak at 281 nm and a shoulder peak at about 317 nm, which is very similar to the excitation band of the PS–Tb fiber membrane in Fig. 10b. Based on the above analysis on the excitation spectrum of the PS–Tb fiber membrane, it can be inferred that the excitation band in Fig. 12a is mainly assigned to the absorption of the organic ligands Phen and AcAc of the Tb^{3+} complex doped in the PS–Eu_1–Tb_{60} fiber membrane. This means that the Tb^{3+} emission in the PS–Eu_1–Tb_{60} fiber membrane is also from the synergistic sensitization of the organic ligands Phen and AcAc in the Tb^{3+} complex. The possible luminescence sensitization process of the Tb^{3+} ions in the PS–Eu_1–Tb_{60} fiber membrane can be described as follows: Phen and AcAc absorb UV light, then transfer the energy to the Tb^{3+} ions, and then the excited state ($^5D_4$) Tb^{3+} ions release the energy in the form of luminescence, which is well known as the "antenna effect".

On the other hand, as shown in Fig. 12b, when monitoring the Eu^{3+} emission at 617 nm, the PS–Eu_1–Tb_{60} fiber membrane exhibits a quite broad excitation band in the range of 240–400 nm with a peak at 300 nm and a shoulder peak at about 375 nm. Based on the above analysis of the excitation spectrum of the PS–Eu fiber membrane in Fig. 9a, it is easy to speculate that the shoulder excitation band in the 350–400 nm range centered at about 375 nm is attributed to the absorption of the organic ligand TTA of the Eu^{3+} complex doped in the PS–Eu_1–Tb_{60} fiber membrane. This result indicates that TTA in the PS–Eu_1–Tb_{60} fiber membrane can sensitize the Eu^{3+} ion luminescence efficiently. In addition, it is noteworthy that the excitation band in the range of 240–350 nm is much stronger than that of the shoulder excitation band in the range of 350–400 nm, which is different from the excitation band of the PS–Eu fiber membrane in Fig. 9a. Moreover, it can be further found that the excitation band of the 240–350 nm range in Fig. 12b overlaps well with the excitation band located at 240–350 nm in Fig. 12a. These phenomena imply that the luminescence sensitization processes of the Eu^{3+} ions in the PS–Eu_1–Tb_{60} fiber membrane (co-doping with the Eu^{3+} complex and the Tb^{3+} complex) might be more complex than in the PS–Eu fiber membrane (single-doping with the Eu^{3+} complex). In fact, in the Eu^{3+}/Tb^{3+} co-doping luminescent systems, the transfer energy from the Tb^{3+} ions to the Eu^{3+} ions usually occurs, which can be supported by the findings of many previous studies.[77,78] Accordingly, it can be inferred that the excitation band of the 240–350 nm range in Fig. 12b might be ascribed to the absorption of the organic ligands (AcAc and Phen) in the Tb^{3+} complex in the PS–Eu_1–Tb_{60} fiber membrane. Except for the sensitization of TTA to the Eu^{3+} ions, the other sensitization process of the Eu^{3+} ions in the PS–Eu_1–Tb_{60} fiber membrane may occur. That is, AcAc and Phen first absorb UV light and transfer the energy to the Tb^{3+} ions, then the excited state ($^5D_4$) Tb^{3+} ions transfer the energy to the Eu^{3+} ions, and finally the excited state ($^5D_0$) Eu^{3+} ions release the energy in the form of luminescence. Here, the energy transfer process from the Tb^{3+} ions to the Eu^{3+} ions is mainly based on the higher energy level of the Tb^{3+} ions ($^5D_4$, 20 500 cm^{-1}) than that of the Eu^{3+} ions ($^5D_0$, 17 300 cm^{-1}).[68,69] Based on the above analysis results, it can be summed up that the Tb^{3+} emission in the PS–Eu_1–Tb_{60} fiber membrane is mainly owing to the sensitization of the organic ligands Phen and AcAc in the Tb^{3+} complex, and the Eu^{3+} emission in the PS–Eu_1–Tb_{60} fiber membrane is mainly due to both the sensitization of the organic ligand TTA in the Eu^{3+} complex and the energy transfer of the Tb^{3+} ions in the Tb^{3+} complex to the Eu^{3+} ions.

By further observing the excitation spectra of the PS–Eu_1–Tb_{60} fiber membrane Fig. 12, it can be found that the excitation intensity at 245 nm is relatively stronger than that at 365 nm when monitoring the 546 nm emission of the Tb^{3+} ions (Fig. 12a), whereas the excitation intensity at 365 nm is relatively stronger than that at 254 nm when monitoring the 617 nm emission of the Eu^{3+} ions (Fig. 12b). The result indicates that the short-wavelength (254 nm) UV light is helpful in exciting the Tb^{3+} ions in the PS–Eu_1–Tb_{60} fiber membrane, while long-wavelength (365 nm) UV light is beneficial to excite the Eu^{3+} ions in the PS–Eu_1–Tb_{60} fiber membrane. It can be confirmed that the primary cause for this result is that the organic ligands Phen and AcAc for sensitizing the Tb^{3+} ions and TTA for sensitizing the Eu^{3+} ions in the PS–Eu_1–Tb_{60} fiber membrane can absorb different wavelength lights, respectively. Thus, the Tb^{3+} ions and the Eu^{3+} ions in the PS–Eu_1–Tb_{60} fiber membrane prefer to be excited by the UV lights close to the absorption wavelengths of their corresponding sensitization ligands. Finally, the PS–Eu_1–Tb_{60} fiber membrane shows UV-excited dual-mode luminescence, *e.g.* green light under 254 nm light irradiation, while red light under 365 nm light irradiation, as presented in Fig. 5. In fact, it can be seen from Fig. 5 that all as-prepared fiber membranes with the different mass ratio of the

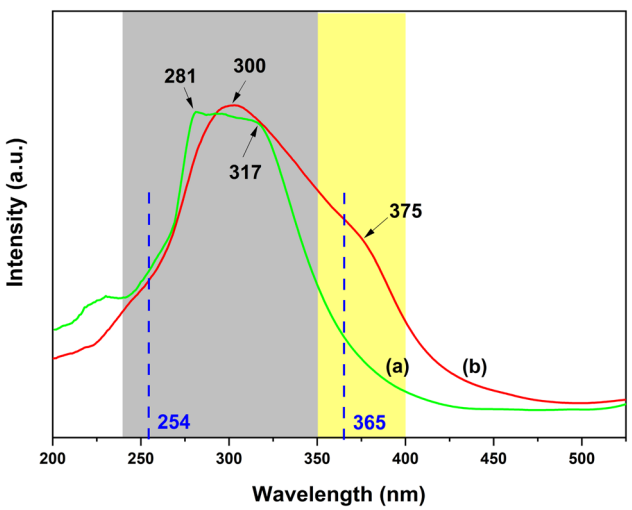

Fig. 12 Excitation spectra of the PS–Eu_1–Tb_{60} fiber membrane by monitoring the Tb^{3+} emission at 546 nm (a) and the Eu^{3+} emission at 617 nm (b), respectively.

Eu^{3+} complex and the Tb^{3+} complex in this work possess the UV-excited dual-mode luminescence properties, and their membrane samples can emit different multicolor lights excited by 254 nm and 365 nm, respectively. These color-switchable multicolor luminescent fiber membranes prepared from waste EPS and the lanthanide complexes can be suitable for designing complex luminescence anti-counterfeiting patterns with high anti-counterfeiting security.

Conclusions

In this work, a simple and effective method to upcycle waste EPS to UV-excited dual-mode multicolor luminescent electrospun fiber membranes for advanced anti-counterfeiting has been successfully developed. This strategy combines the excellent spinnability of the recycled PS and the unique luminescence properties of the Eu^{3+} complex and the Tb^{3+} complex under UV lights. The as-prepared fiber membranes exhibit excellent UV-excited dual-mode luminescent properties due to the organic ligands sensitizing the Tb^{3+} ions and the Eu^{3+} ions can absorb different wavelength UV lights, respectively. The luminescence colors of the fiber membranes can be easily fine-tuned by adjusting the mass ratio of the two lanthanide complexes and switching the irradiation wavelengths (254 nm or 365 nm) of the UV light sources. Using these fiber membranes with tunable multicolor luminescence, complex luminescence anti-counterfeiting patterns can be constructed. Noteworthy, the 254 nm and 365 nm light sources are two of the most used commercial UV light sources. These results demonstrate that the UV-excited dual-mode multicolor luminescent fiber membranes prepared from waste EPS in this work are highly promising for advanced anti-counterfeiting and encryption applications. Moreover, the strategy of co-doping the Eu^{3+} complex and Tb^{3+} complex into a recycled polymer in this work could be further extended to upcycling other waste plastics and developing new UV-excited dual-mode luminescent anti-counterfeiting functional fiber membranes, films or polymeric gels, and so on.

Conflicts of interest

There are no conflicts to declare.

Acknowledgements

This work was funded by the National Natural Science Foundation of China (No. 22275074), Key R&D Program of Zhejiang Province (No. 2023C01199), Zhejiang Province Commonweal Technique Research Project (2017C33031) and Jiaxing Public Welfare Research Project (No. 2021AY10070). This work was also supported by the Cultivation Plan of the General Program of the National Natural Science Foundation of China (No. 00321069).

Notes and references

1 X. Li, L. Jin and H. Kan, *Nature*, 2019, **570**, 437–439.
2 X. Wang, A. Mahmood, G. H. Lu, X. F. Xie and J. Sun, *Chem. Eng. J.*, 2020, **450**, 138168.
3 D. Wood, S. Shaw, T. Cawte, E. Shanen and B. V. Heyst, *Chem. Eng. J.*, 2020, **391**, 123490.
4 M. M. Li, Q. Cheng, C. Shen, B. Hong, Y. Jiang, Y. X. Wei, M. D. Cai, J. S. Chen and S. Sun, *RSC Adv.*, 2022, **12**, 22410–22415.
5 L. I. Qrenawi and F. K. J. Rabah, *J. Membr. Sci. Res.*, 2023, **9**, 548826.
6 Z. Z. Zhu, Z. Chen, X. Luo, W. X. Zhang and S. J. Meng, *Chem. Eng. J.*, 2020, **399**, 125650.
7 C. L. Xia, X. Li, Y. J. Wu, S. Suharti, Y. Unpaprom and A. Pugazhendhi, *Environ. Res.*, 2023, **222**, 115318.
8 W. X. Zhang and F. Jiang, *Water Res.*, 2019, **157**, 445–453.
9 D. M.-C. Chen, B. L. Bodirsky, T. Krueger, A. Mishra and A. Popp, *Environ. Res. Lett.*, 2020, **15**, 074021.
10 H. M. Hou, L. J. Su, D. F. Guo and H. Xu, *J. Cleaner Prod.*, 2023, **383**, 135449.
11 N. Singh, D. Hui, R. Singh, I. P. S. Ahuja, L. Feo and F. Fraternali, *Composites, Part B*, 2017, **115**, 409–422.
12 A. K. Panda, R. K. Singh and D. K. Mishra, *Renewable Sustainable Energy Rev.*, 2010, **14**, 233–248.
13 N. Chaukura, W. Gwenzi, T. Bunhu, D. T. Ruziwa and I. Pumure, *Resour., Conserv. Recycl.*, 2016, **107**, 157–165.
14 Z. Xu, F. P. Pan, M. Q. Sun, J. J. Xu, N. E. Munyaneza, Z. L. Croft, G. S. Cai and G. L. Liu, *Proc. Natl. Acad. Sci. U. S. A.*, 2022, **119**, e2203346119.
15 Z. G. Wang, C. L. Song, Y. M. Qiao, Y. Wu, Z. Z. Yang, H. F. Lu, A. H. Xu, S. Gao and F. Liu, *Polymer*, 2023, **267**, 125666.
16 W. Li, Z. F. Xie, S. S. Xue, H. Ye, M. Y. Liu, W. Shi and Y. C. Liu, *Sep. Purif. Technol.*, 2021, **11**, 119435.
17 M. Y. Liu, Z. F. Xie, H. Ye, W. Li, W. Shi, Y. C. Liu and Y. Zhang, *Colloids Surf., A*, 2021, **627**, 127155.
18 J. Z. Jia, Z. Y. Fu, L. Wang, Z. N. Huang and C. K. Liu, *Chem. Eng. Res. Des.*, 2019, **142**, 346–354.
19 F. Maleki, H. Mashhadimoslem, A. Ghaemi and G. M. M. Sadeghi, *Mater. Chem. Phys.*, 2022, **292**, 126779.
20 G. Gatti, M. Errahali, L. Tei, E. Mangano, S. Brandani, M. Cossi and L. Marchese, *Nanomaterials*, 2019, **9**, 726.
21 N. C. F. Machado, L. A. M. de Jesus, P. S. Pinto, F. G. F. de Paula, M. O. Alves, K. H. A. Mendes, R. V. Mambrini, D. Barrreda, V. Rocha, R. Santamaría, J. P. C. Trigueiro, R. L. Lavall and P. F. R. Ortega, *J. Cleaner Prod.*, 2021, **313**, 127903.
22 N. Deka, J. Barman, S. Kasthuri, V. Nutalapati and G. K. Dutta, *Appl. Surf. Sci.*, 2020, **511**, 145576.
23 Y. X. Zhang, Z. M. Shen, Y. F. Yu, L. Liu, G. X. Wang and A. B. Chen, *J. Mater. Sci.*, 2018, **53**, 12115–12122.
24 T. Q. Zhao, X. H. Tan, L. T. Song, L. M. Guo, Y. L. Liu, X. H. Kang, X. M. Meng, H. F. Wang and W. G. Chu, *ACS Appl. Energy Mater.*, 2020, **3**, 9369–9378.
25 J. L. Andres, R. D. Hersch, J.-E. Moser and A.-S. Chauvin, *Adv. Funct. Mater.*, 2014, **24**, 5029–5036.
26 L. Ju, W. B. Gao, J. Y. Zhang, T. Y. Qin, Z. Du, L. Sheng and S. X.-A. Zhang, *J. Mater. Chem. C*, 2020, **8**, 2806–2811.

27 M. Y. Pan, L. B. Wang, S. L. Dou, J. P. Zhao, H. B. Xu, B. Wang, L. P. Zhang, X. B. Li, L. Pan and Y. Li, *Crystals*, 2019, **9**, 417.
28 Y. Sun, X. X. Le, S. Y. Zhou and T. Chen, *Adv. Mater.*, 2022, **34**, 2201262.
29 P. Kumar, S. Singh and B. K. Gupta, *Nanoscale*, 2016, **8**, 14297–14340.
30 X. W. Yu, H. Y. Zhang and J. H. Yu, *Aggregate*, 2021, **2**, 20–34.
31 H. Yin, Y.-M. Zhang, H.-F. Zhao, G.-J. Yang, Y. Shi, S. X.-A. Zhang and D.-J. Ding, *Dyes Pigm.*, 2018, **159**, 506–512.
32 J. Yuan, P. R. Christensen and M. O. Wolf, *Chem. Sci.*, 2019, **10**, 10113–10121.
33 J. Wu, X. J. Zhou, D. Zhang, L. Li, S. Jiang, G. T. Xiang, Y. J. Wang, X. Tang, J. F. Li and Z. M. Cao, *J. Lumin.*, 2023, **257**, 119686.
34 R. Shi, L. Yu, Y. R. Tian, X. M. Wang, Z. Y. Sun, B. Qi and F. Luo, *Mater. Chem. Phys.*, 2022, **280**, 125806.
35 H. Suo, Q. Zhu, X. Zhang, B. Chen, J. K. Chen and F. Wang, *Mater. Today Phys.*, 2021, **21**, 100520.
36 Y. L. Liu, K. L. Ai and L. H. Lu, *Nanoscale*, 2011, **3**, 4804–4810.
37 J. Z. Guo, H. Li, L. T. Ling, G. Li, R. Cheng, X. Lu, A.-Q. Xie, Q. Li, C.-F. Wang and S. Chen, *ACS Sustainable Chem. Eng.*, 2020, **8**, 1566–1572.
38 K. Jiang, L. Zhang, J. F. Lu, C. X. Xu, C. Z. Cai and H. W. Lin, *Angew. Chem.*, 2016, **128**, 7347–7351.
39 L. M. Xu, J. W. Chen, J. Z. Song, J. H. Li, J. Xue, Y. H. Dong, B. Cai, Q. S. Shan, B. N. Han and H. B. Zeng, *ACS Appl. Mater. Interfaces*, 2017, **9**, 26556–26564.
40 X. Li, S. H. Xu, F. Liu, J. F. Qu, H. B. Shao, Z. Y. Wang, Y. P. Cui, D. Y. Ban and C. L. Wang, *ACS Appl. Mater. Interfaces*, 2021, **13**, 31031–310370.
41 J. Kido and Y. Okamoto, *Chem. Rev.*, 2002, **102**, 2357–2368.
42 P. Li and H. R. Li, *Coord. Chem. Rev.*, 2021, **441**, 213988.
43 M. P. Dandekar, S. G. Itankar, S. B. Kondawar, D. V. Nandanwar and P. Koinkar, *Opt. Mater.*, 2018, **85**, 483–490.
44 X. P. Zhang, S. P. Wen, S. Hu, L. Q. Zhang and L. Liu, *J. Rare Earths*, 2010, **28**, 333–339.
45 H. Q. Yu, Y. Li, T. Li, B. J. Chen, P. Li and Y. B. Wu, *Russ. J. Phys. Chem. A*, 2015, **89**, 2455–2460.
46 Y. Li, D. S. Li, E. Y. B. Pun and H. Lin, *Opt. Mater.*, 2018, **84**, 38–45.
47 H. Kara, G. Oylumluoglu and M. B. Coban, *J. Cluster Sci.*, 2020, **31**, 701–708.
48 P. Philip, P. Thomas, E. T. Jose, K. C. Philip and P. C. Thomas, *Bull. Mater. Sci.*, 2019, **42**, 218.
49 X.-Q. Song, H.-H. Meng, Z.-G. Lin and L. Wang, *ACS Appl. Polym. Mater.*, 2020, **2**, 1644–1655.
50 H. G. Wang, Q. B. Yang, L. Sun, C. Q. Zhang, Y. C. Li, S. Wang and Y. X. Li, *J. Alloys Compd.*, 2009, **488**, 414–419.
51 Y. Li, C.-Y. Zhang, D.-G. Yu and X. Wang, *RSC Adv.*, 2016, **6**, 84074–84081.
52 E. S. Andreiadis, N. Gauthier, D. Imbert, R. Demadrille, J. Pécaut and M. Mazzanti, *Inorg. Chem.*, 2013, **52**, 14382–14390.
53 Y. X. Zhu, G. C. Pan, J. Zhao, K. L. Liu, W. F. Xue, Y. Q. Wang, W. W. You, H. P. Gao, W. Xu and Y. L. Mao, *Adv. Opt. Mater.*, 2022, **11**, 2202019.
54 Y. H. Dong, H. R. Zhao, S. P. Wang, Q. Cheng, S. X. Liu and Y. Li, *ACS Appl. Mater. Interfaces*, 2022, **14**, 40313–40321.
55 W. J. Liu, W. J. Zhang, G. J. Li and R. X. Liu, *Dalton Trans.*, 2021, **50**, 10243–10251.
56 A. Tymiński, E. Śmiechowicz, I. R. Martín and T. Grzy, *ACS Appl. Nano Mater.*, 2020, **3**, 6541–6551.
57 A. Szczeszak, M. Skwierczyńska, D. Przybylska, M. Runowski, E. Śmiechowicz, A. Erdman, O. Ivashchenko, T. Grzyb, P. Kulpiński and K. Olejnik, *Mater. Des.*, 2022, **218**, 110684.
58 A. K. Singh, S. Singh and B. K. Gupta, *ACS Appl. Mater. Interfaces*, 2018, **10**, 44570–44575.
59 M. X. Li, Y. Feng, Q. Y. Tian, W. J. Yao, L. Liu, X. Li, H. J. Wang and W. Wu, *Dalton Trans.*, 2018, **47**, 11264–11271.
60 B. Chen, H. P. Xie, S. Wang, Z. Y. Guo, Y. F. Hu and H. Z. Xie, *Luminescence*, 2019, **34**, 437–443.
61 H. Fong, I. Chun and D. H. Reneke, *Polymer*, 1999, **40**, 4585–4592.
62 S.-H. Tan, R. Inai, M. Kotaki and S. Ramakrishna, *Polymer*, 2005, **46**, 6128–6134.
63 R. Ishimatsu, E. Kunisawa, K. Nakano, C. Adachi and T. Imato, *ChemistrySelect*, 2019, **4**, 2815–2831.
64 E. Regalado-Pérez, N. R. Mathews and X. Mathew, *Sol. Energy*, 2020, **199**, 82–91.
65 L. U. Khan, H. F. Brito, J. Hölsä, K. R. Pirota, D. Muraca, M. C. F. C. Felinto, E. E. S. Teotonio and O. L. Malta, *Inorg. Chem.*, 2014, **53**, 12902–12910.
66 D. Liu, Y.-N. Zhou, J. L. Zhao, Y. L. Xu, J. F. Shen and M. G. Wu, *J. Mater. Chem. C*, 2017, **5**, 11620–11630.
67 M. Latva, H. Takalo, V.-M. Mukkala, C. Matachescu, J. C. Rodriguez-Ubis and J. Kankare, *J. Lumin.*, 1997, **75**, 149–169.
68 Y. L. Guo, W. Dou, X. Y. Zhou, W. S. Liu, W. W. Qin, Z. P. Zang, H. R. Zhang and D. Q. Wang, *Inorg. Chem.*, 2009, **48**, 3581–3590.
69 C. Feng, J.-W. Sun, P.-F. Yan, Y.-X. Li, T.-Q. Liu, Q.-Y. Sun and G.-M. Li, *Dalton Trans.*, 2015, **44**, 4640–4647.
70 V. Divya, S. Biju, R. Luxmi Varma and M. L. P. Reddy, *J. Mater. Chem.*, 2010, **20**, 5220–5227.
71 S. Biju, D. B. Ambili Raj, M. L. P. Reddy and B. M. Kariuki, *Inorg. Chem.*, 2006, **45**, 10651–10660.
72 J. Zhang, J. L. Shen and X. G. Huang, *J. Mater. Sci.: Mater. Electron.*, 2015, **26**, 7263–7269.
73 W.-D. Liu, G.-J. Li, H. Xu, M.-H. Du, L.-S. Long, L.-S. Zheng and X.-J. Kong, *Inorg. Chem.*, 2022, **61**, 9849–9854.
74 Y. X. Zheng, J. Lin, Y. J. Liang, Q. Lin, Y. N. Yu, Q. G. Meng, Y. H. Zhou, S. B. Wang, H. Y. Wang and H. J. Zhang, *J. Mater. Chem.*, 2001, **11**, 2615–2619.
75 L. Prodi, M. Maestri, R. Ziessel and V. Balzani, *Inorg. Chem.*, 1991, **30**, 3798–3802.
76 S. Raphael, M. L. P. Reddy, A. H. Cowley and M. Findlater, *Eur. J. Inorg. Chem.*, 2008, **2008**, 4387–4394.
77 X. Xu, H. L. Li, S. S. Xie, L. Mei, R. Meng, L. J. Chen and J. W. Zhao, *Inorg. Chem.*, 2020, **59**, 648–660.
78 A. R. Ramya, D. Sharma, S. Natarajan and M. L. P. Reddy, *Inorg. Chem.*, 2012, **51**, 8818–8826.